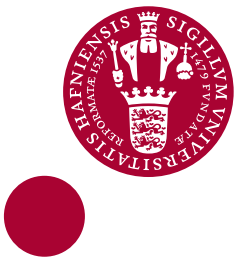

Episodic formation of refractory inclusions in the Solar System and their presolar heritage

Larsen, K. K.; Wielandt, D.; Schiller, M.; Krot, A. N.; Bizzarro, M.

Published in:
Earth and Planetary Science Letters

DOI:
10.1016/j.epsl.2020.116088

Publication date:
2020

Document version
Publisher's PDF, also known as Version of record

Earth and Planetary Science Letters 535 (2020) 116088

Contents lists available at ScienceDirect

Earth and Planetary Science Letters

www.elsevier.com/locate/epsl

Episodic formation of refractory inclusions in the Solar System and their presolar heritage

K.K. Larsen [a,*], D. Wielandt [a], M. Schiller [a], A.N. Krot [a,b], M. Bizzarro [a]

[a] Centre for Star and Planet Formation, Natural History Museum of Denmark, University of Copenhagen, Copenhagen DK-1350, Denmark
[b] Hawai'i Institute of Geophysics and Planetology, University of Hawai'i at Manoa, HI 96822, USA

ARTICLE INFO

Article history:
Received 28 April 2019
Received in revised form 18 December 2019
Accepted 9 January 2020
Available online 28 January 2020
Editor: R. Dasgupta

Keywords:
Solar System formation
refractory inclusion
Mg isotope
episodic outburst
^{26}Al
presolar dust

ABSTRACT

Refractory inclusions [Ca-Al-rich Inclusions (CAIs) and Amoeboid Olivine Aggregates (AOAs)] in primitive meteorites are the oldest Solar System solids. They formed in the hot inner protoplanetary disk and, as such, provide insights into the earliest disk dynamics and physicochemical processing of the dust and gas that accreted to form the Sun and its planetary system. Using the short-lived ^{26}Al to ^{26}Mg decay system, we show that bulk refractory inclusions in CV (Vigarano-type) and CR (Renazzo-type) carbonaceous chondrites captured at least two distinct ^{26}Al-rich (^{26}Al/^{27}Al ratios of $\sim 5 \times 10^{-5}$) populations of refractory inclusions characterized by different initial ^{26}Mg/^{24}Mg isotope compositions ($\mu^{26}Mg^*_0$). Another ^{26}Al-poor CAI records an even larger $\mu^{26}Mg^*_0$ deficit. This suggests that formation of refractory inclusions was punctuated and recurrent, possibly associated with episodic outbursts from the accreting proto-Sun lasting as short as <8000 yr. Our results support a model in which refractory inclusions formed close to the hot proto-Sun and were subsequently redistributed to the outer disk, beyond the orbit of Jupiter, plausibly via stellar outflows with progressively decreasing transport efficiency. We show that the magnesium isotope signatures in refractory inclusions mirrors the presolar grain record, demonstrating a mutual exclusivity between ^{26}Al enrichments and large nucleosynthetic Mg isotope effects. This suggests that refractory inclusions formed by incomplete thermal processing of presolar dust, thereby inheriting a diluted signature of their isotope systematics. As such, they record snapshots in the progressive sublimation of isotopically anomalous presolar carriers through selective thermal processing of young dust components from the proto-Solar molecular cloud. We infer that ^{26}Al-rich refractory inclusions incorporated ^{26}Al-rich dust which formed <5 Myr prior to our Sun, whereas ^{26}Al-poor inclusions (such as FUN- and PLAC-type CAIs) incorporated >10 Myr old dust.

1. Introduction

Our Solar System formed through the collapse of a well-mixed molecular cloud core made up of dust and gas originating from a multitude of nucleosynthetic sources (Vasileiadis et al., 2013; Kuffmeier et al., 2016). This nucleosynthetic diversity is preserved in presolar grains from primitive meteorites. Through gravitational core collapse, the earliest energetic phase of protostellar evolution was characterized by high mass accretion rates onto the forming proto-Sun ($\sim 10^{-5}$ $M_\odot$ yr^{-1}) (D'Alessio et al., 2005), punctuated by protostellar episodic outbursts (Frimann et al., 2016; Hsieh et al., 2018). This resulted in a very hot inner protoplanetary disk. Based on their high-temperature mineralogy and irradiation signatures (Wielandt et al., 2012; Sossi et al., 2017), refractory inclusions [Ca-Al-rich Inclusions (CAIs) and Amoeboid Olivine Aggregates (AOAs)] are thought to have condensed at this stage from a gas in the innermost region of the protoplanetary disk (Scott and Krot, 2014). As such, CAIs from CV (Vigarano-type) carbonaceous chondrites record an absolute age of 4,567.30 ± 0.16 Myr (Connelly et al., 2012), defining the onset of our Solar System. Hence, refractory inclusions captured the earliest physicochemical processing of the presolar dust that accreted to form the Sun and its planetary system.

Our understanding of the formation of refractory inclusions primarily comes from petrographic, chemical, and isotopic analysis of the large, mm- to cm-sized CAIs in CV chondrites (MacPherson, 2014). Except for a few rare refractory inclusions, CV CAIs and AOAs generally exhibit excesses in ^{26}Mg that correlate with their ^{27}Al/^{24}Mg ratio, signifying the former presence of short-lived radioactive ^{26}Al with an initial $(^{26}Al/^{27}Al)_0$ ratio of $(5.25 \pm 0.02) \times 10^{-5}$ (Larsen et al., 2011). This has been interpreted to reflect formation of these inclusions within less than ~ 8000 yr from a

* Corresponding author.
E-mail address: kirstenla@live.dk (K.K. Larsen).

https://doi.org/10.1016/j.epsl.2020.116088

CAI-forming gas enriched in ^{26}Al via chemical processing of ^{26}Al-rich presolar carriers (Larsen et al., 2011). The idea of enrichment of ^{26}Al in the CAI-forming reservoir is supported by correlated minor enrichments in neutron-rich isotopes of the iron peak elements (^{48}Ca, ^{50}Ti, ^{54}Cr) in ^{26}Al-rich CV CAIs; interpreted to be the result of selective thermal processing of isotopically anomalous presolar carriers (Trinquier et al., 2009; Larsen et al., 2011; Schiller et al., 2015, 2018). Much larger nucleosynthetic effects are known to exist in ^{26}Al-poor FUN/UN-type (Fractionation and Unidentified Nuclear effects) CAIs from CV chondrites, as well as ^{26}Al-poor PLAC-type CAIs (PLAty hibonite Crystals) from CM chondrites, indicating residual nucleosynthetic variability in some refractory inclusions (Ireland, 1990; Liu et al., 2009; Kööp et al., 2016; 2018). This has been proposed to result from incomplete chemical homogenization of isotopically diverse presolar dust components and that refractory inclusions, contrary to current belief, did not form exclusively from a single, completely homogenized gas of solar composition (Ireland, 1990). These observations are not compatible with complete sublimation of all presolar material into a gaseous state prior to CAI-formation. As such, it is not clear if the ^{26}Al-^{26}Mg isotope systematics of ^{26}Al-rich CV-type CAIs and AOAs are representative for refractory inclusions in other types of carbonaceous chondrites or if they merely represent a snapshot of isotopically evolving protoplanetary gas and dust reservoirs.

It is well known that features such as size, type, mineralogy and abundance of refractory inclusions differ between different groups of carbonaceous chondrites (Scott and Krot, 2014), which are believed to have accreted at various heliocentric distances from the Sun in the outer Solar System (Warren, 2011). For example, in CR chondrites (Renazzo-type carbonaceous chondrites) refractory inclusions are typically very small (10–300 μm), about an order of magnitude less abundant (<1 vol%) than in CV chondrites and on average mineralogically distinct (Krot et al., 2002). Thus, it is conceivable that their isotope systematics also record differences in their formation conditions and reveal whether refractory inclusions in different chondrite groups represent distinct populations with unique isotope signatures. Importantly, CR chondrites are some of the most pristine early Solar System materials that escaped secondary asteroidal thermal metamorphism and experienced only minor aqueous alteration (Krot et al., 2002; Makide et al., 2009). As such, CR CAIs represent ideal targets to search for primordial isotopic differences to other CAIs that is associated with their formation process. Here, we report on the first high-precision Multiple-Collector Inductively-Coupled-Plasma source Mass-Spectrometry (MC-ICPMS) magnesium isotope analysis of 17 bulk refractory inclusions [including six AOAs, five fine-grained spinel-rich (FG) CAIs and six CAIs with evidence for partial or complete melting] from five CR chondrites, as well as three additional FG CAIs from the reduced CV chondrite Efremovka and mineral fractions from the KT-1 FUN-type CV CAI (Thrane et al., 2008).

2. Materials and methods

Petrographic characterization of refractory inclusions was carried out using the JEOL JXA-8500F Field Emission electron microprobe and JEOL JSM-5900LV scanning electron microscope (SEM) equipped with an energy-dispersive X-ray spectrometer (EDS) at the University of Hawaii at Manoa, as well as the Phillips XL40 SEM equipped with EDS located at the Geological Survey of Denmark and Greenland (GEUS) in Copenhagen. Given the very low abundance of refractory inclusions in CR2 chondrites (typically <1 vol%) (Scott and Krot, 2014), a systematic survey for refractory inclusions in a range of pristine CR2 chondrites was carried out based on combined X-ray elemental maps (Mg – red, Ca – green, and Al – blue) of polished meteorite sections. The X-ray elemental maps in Mg, Ca, Al, Ti and Na K α were acquired with JEOL JXA-8500F using a 15 keV accelerating voltage, 50–100 nA beam current, and a beam size of ~1 μm.

A subset of larger inclusions from five CR2 chondrites [North West Africa (NWA) 6043, NWA 7837, NWA 7655, Elephant Moraine (EET) 92161, Graves Nunataks (GRA) 95229] and one reduced CV3 chondrite (Efremovka) was selected for sampling and isotope analysis. Sampling was performed using the New Wave Research MicroMill at the Centre for Star and Planet Formation, University of Copenhagen, equipped with tungsten carbide (WC) or diamond coated microdrill bits (200–500 μm) by drilling into a small droplet of MilliQ water and extracting the sample using a thin, elongated custom made Pasteur pipette. Samples were then transferred to small pre-cleaned Savillex PFA Teflon beakers in preparation for digestion in ultra-clean distilled acids prior to chromatographic purification following the procedures outlined in Larsen et al., 2018. In brief, samples were digested in a mixture of concentrated HF:HNO_3 (3:1) for 2 days at 120 °C, followed by digestion in aqua regia (HCl(3):HNO_3 (1)) for 2 days at 120 °C and conversion to NO_3-salts through two evaporation-cycles with HNO_3. All chemical procedures were performed in an ultra-clean laboratory environment using double distilled acids and distilled MilliQ water. Ion chromatographic purification of Mg was performed using a series of cation and anion exchange resins (AG50w-x8, TODGA, Ni-spec) as described in detail in Larsen et al., 2018.

Magnesium-isotope analysis was performed using the Thermo-Finnigan Neptune Plus Multiple-Collector Inductively-Coupled-Plasma source Mass-Spectrometer (MC-ICP-MS) located at the Centre for Star and Planet Formation (Natural History Museum of Denmark, University of Copenhagen), following procedure outlined in Bizzarro et al., 2011 and Larsen et al., 2018. In brief, purified Mg was introduced into the plasma source by means of an Apex IR desolvating nebulizer in a 2% HNO_3 run solution at 50 ml min^{-1} using a Thermo Fisher Jet sample cone and skimmer X-cone interface in high-resolution mode. Corrections for instrumental mass bias were obtained by sample–standard bracketing with sample/standard peak intensities matching to better than 5%. Samples and standards were analyzed 10 times with each analysis consisting of 100 cycles of 16.78 second integrations separated by a total of 822 seconds of on-peak zero blank measurements in clean 2% HNO_3 solution.

Stable magnesium isotope ratios are reported in parts per million (ppm) deviation relative to the composition of the Mg reference standard DTS-2B (Olsen et al., 2013) according to: $\mu^{25}Mg = [(^{25}Mg/^{24}Mg)_{sample}/(^{25}Mg/^{24}Mg)_{DTS\text{-}2B} - 1] \times 10^6$. The mass-independent $\mu^{26}Mg^*$ (non-radiogenic ^{26}Mg + radiogenic ^{26}Mg ingrowth from ^{26}Al decay) is reported in the same fashion after mass bias correction using the exponential fractionation law and internal normalization to $^{25}Mg/^{24}Mg = 0.126896$ (Bizzarro et al., 2011). Data reduction was conducted offline using the software package Iolite (Paton et al., 2011) and is reported in Table 1.

$^{27}Al/^{24}Mg$ ratios were determined using the Thermo Fisher Scientific quadrupole ICP-MS located at the Centre for Star and Planet Formation (Natural History Museum of Denmark, University of Copenhagen), by standard-sample bracketing on sample-matched gravimetric standards with $^{27}Al/^{24}Mg$ ratios of 0.1, 1.3, 3.4 and 5.7, thereby covering the range of $^{27}Al/^{24}Mg$ ratios for refractory inclusions reported in this study. Repeat measurements of two basaltic USGS standards (BHVO-2 and BCR-2) and two CAIs (Cp1 and Cp2) showed that accurate $^{27}Al/^{24}Mg$ ratios, as compared to spiked $^{27}Al/^{24}Mg$ ratios reported in Paton et al., 2012 and nominal USGS values, can be obtained to a precision of <2% (Fig. S1). Data reduction was conducted using the software package Iolite (Paton et al., 2011).

Table 1
Mg isotope data for refractory inclusions in CR2 and CV3 chondrites.

Sample ID	Meteorite	Type of inclusion	μ^{25}Mg	2se	μ^{26}Mg*	2se	*n*	^{27}Al/^{24}Mg	2se
CV3 inclusions									
EK14	Efremovka ($CV3_{red}$)	Fine-grained CAI	181	12	305.9	2.6	8	0.856	0.017
EK12	Efremovka ($CV3_{red}$)	Fine-grained CAI	−580	4	542.6	3.4	10	1.480	0.030
EK3	Efremovka ($CV3_{red}$)	Fine-grained spinel-rich CAI	−370	4	989.0	3.4	10	2.955	0.059
CR2 inclusions									
NWA6043-2b-#9	NWA 6043 (CR2)	AOA	105	4	10.3	3.1	10	0.061	0.002
NWA6043-2b-#6	NWA 6043 (CR2)	AOA	−457	5	18.6	3.8	10	0.049	0.002
GRA-#3	GRA 95229 (CR2)	AOA	−101	5	18.7	2.8	10	0.086	0.003
NWA7837-D#2	NWA 7837 (CR/CV?)	AOA	−88	5	52.1	2.9	10	0.169	0.007
GRA-#1	GRA 95229 (CR2)	AOA	−193	5	126.9	5.0	10	0.295	0.012
NWA6043-2b-#l	NWA 6043 (CR2)	AOA	−151	3	127.9	2.2	10	0.271	0.011
NWA6043-l-#3	NWA 6043 (CR2)	Fine-grained CAI	−28	3	164.6	2.2	10	0.763	0.069
NWA7837-D#3	NWA 7837 (CR/CV?)	Fine-grained CAI	467	6	419.3	2.4	10	1.391	0.028
NWA6043-0A-#17	NWA 6043 (CR2)	Fine-grained CAI	551	1	548.4	2.0	8	1.704	0.068
NWA7655-P6	NWA 7655 (CR2)	Fine-grained CAI	805	5	563.9	5.3	3	1.799	0.036
NWA6043-0A-# 11	NWA 6043 (CR2)	Flyffy type A CAI	−69	17	764.2	4.8	6	2.488	0.149
EET921 61-18a-#l	EET 92161 (CR2)	Fine-grained spinel-rich CAI	606	10	967.1	2.9	10	2.930	0.059
NWA7837-D#1	NWA 7837 (CR/CV?)	Type B CAI	6780	4	1005.2	4.1	10	3.013	0.060
NWA6043-2A-#2	NWA 6043 (CR2)	Sp-rich CAI	1840	11	1010.7	0.4	3	2.903	0.058
N-53	NWA 6043 (CR2)	Compound type B/C CAI	4902	7	1022.3	7.6	10	2.942	0.059
NWA6043-l-#6	NWA 6043 (CR2)	Melilite-rich CTA CAI	4738	3	1388.5	2.3	10	3.979	0.080
NWA6043-1 A-#8	NWA 6043 (CR2)	Hib-rich CAI	−98	4	1696.6	5.7	3	5.108	0.102
KT-I FUN CV CAI mineral fractions									
KT-f5	NWA 779 (CV3)	FUN CAI, spinel-rich mineral fragment	39630	9	−387.9	3.9	7	3.101	0.124
KT-f6	NWA 779 (CV3)	FUN CAI, spinel + melilite-rich mineral fragment	35977	51	−368.4	5.1	3	3.362	0.134
KT-fl	NWA 779 (CV3)	FUN CAI, melilite-rich mineral fragment	34300	2	−277.0	4.4	3	4.617	0.462
KT-f3	NWA 779 (CV3)	FUN CAI, melilite-rich mineral fragment	36082	11	−302.2	5.8	1	5.166	0.155

3. ^{26}Al-^{26}Mg isotope systematics of refractory inclusions from CR and CV chondrites

In the ^{26}Al-^{26}Mg isochron diagram, two FG CV CAIs (EK12 and EK14) plot on the bulk CV CAI-AOA isochron [$(^{26}Al/^{27}Al)_0 = (5.252 \pm 0.019) \times 10^{-5}$, $\mu^{26}Mg^*_0 = -15.9 \pm 1.4$ ppm] previously determined for refractory inclusions in the reduced CV chondrite Efremovka (Larsen et al., 2011), while all of the CR CAIs and one FG CV CAI (EK3) plot consistently below it (Fig. 1a). Three of the CR AOAs plot on the CV isochron, while another three CR AOAs plot slightly above it. Refining the CV isochron using the old data including the two new FG CV CAIs results in an isochron with a $(^{26}Al/^{27}Al)_0$ ratio of $(5.252 \pm 0.018) \times 10^{-5}$ and $\mu^{26}Mg^*_0$ of -15.9 ± 1.4 ppm (MSWD = 0.98), i.e. identical to that reported in Larsen et al., 2011. A regression solely using bulk CV CAIs (i.e. excluding AOAs) also defines an isochron with an indistinguishable $(^{26}Al/^{27}Al)_0$ ratio of $(5.26 \pm 0.05) \times 10^{-5}$ and intercept of $\mu^{26}Mg^*_0 = -17.8 \pm 9.6$ ppm. This is distinct from the isochron intercept of −34 ppm predicted for a homogeneous distribution of ^{26}Al in the Solar protoplanetary disk (Kita et al., 2013). Mineral fractions from the KT-1 FUN CV CAI record significant deficits in μ^{26} Mg* corresponding to a $\mu^{26}Mg^*_0$ value of -545 ± 300 ppm with no evidence for the former presence of ^{26}Al, i.e. $(^{26}Al/^{27}Al)_0$ of $(0.7 \pm 1.0) \times 10^{-5}$ (Fig. 1a).

Fine-grained spinel-rich CV and CR refractory inclusions have textural and mineralogical characteristics consistent with their primary condensation origin, which is also corroborated by the pristine internal isochrons for FG CV CAIs [average $(^{26}Al/^{27}Al)_0$ ratio of $(5.1 \pm 0.2) \times 10^{-5}$ (MacPherson et al., 2012)], i.e., consistent with the $(^{26}Al/^{27}Al)_0$ ratio defined by bulk CV CAIs. Other, typically coarse-grained igneous CAI types record $(^{26}Al/^{27}Al)_0$ ratios as low as $\sim 4.3 \times 10^{-5}$, suggesting their later resetting up to ~200,000 yr after formation of FG CAIs (MacPherson et al., 2012). CR CAIs are typically fragmented in nature such that individual fragments may not reflect their true bulk ^{26}Al-^{26}Mg isotope systematics (Simon and Grossman, 2006), especially for coarse-grained igneous CAIs. Therefore, we restrict our analysis to the five fine-grained CR CAIs to constrain the primary condensation history for CR CAIs. An isochron using these data results in an $(^{26}Al/^{27}Al)_0$ ratio of $(5.1 \pm 0.2) \times 10^{-5}$, consistent with the bulk CV isochron and internal isochrons for CR CAIs recording $(^{26}Al/^{27}Al)_0$ of ~(4.4–5.4) $\times 10^{-5}$ (Makide et al., 2009), but with lower initial $\mu^{26}Mg^*_0$ of −95 ± 26 ppm, i.e. 79 ± 26 ppm lower than the CV isochron. Four of the re-molten CR CAIs analyzed here are not well-constrained by the CR isochron, a feature that we attribute to their fragmental nature and, hence, unrepresentative sampling of their bulk composition as mentioned above.

While the initial $\mu^{26}Mg^*_0$ values determined from internal ^{26}Al-^{26}Mg CAI isochrons measured by secondary ion mass-spectrometry are generally poorly constrained, one CR CAI [with the inferred $(^{26}Al/^{27}Al)_0$ of $(5.4 \pm 0.6) \times 10^{-5}$] shows a resolvable $\mu^{26}Mg^*_0$ deficit of −400 ± 300 ppm (Makide et al., 2009), i.e. within error of the bulk CR CAI isochron. Moreover, a high-precision internal isochron for a type B CV CAI ('Egg-3'; Wasserburg et al., 2012) has identical $(^{26}Al/^{27}Al)_0$ and $\mu^{26}Mg^*_0$ to the CR isochron (Fig. 1a). Similarly, a few FoB (Forsterite-rich type B) CAIs (MacPherson et al., 2016) record identical $\mu^{26}Mg^*_0$ values within error to that defined here for CR CAIs. We further note that another bulk CV CAI (EK3) measured in this study plots on the CR isochron. When comparing the isochron intercepts, $\mu^{26}Mg^*_0$, versus their slope, ^{26}Al/^{27}Al, for these inclusions, (Fig. 1b) it is evident that the ^{26}Al-^{26}Mg isotope composition of such CV and CR CAIs cannot be explained by their formation from an evolving reservoir constrained by the CV isochron. Instead they must have formed from a reservoir characterized by non-Solar Mg-isotope composition with a lower $\mu^{26}Mg^*_0$ similar to that defined here for CR CAIs (unrelated to radiogenic decay of ^{26}Al). Thus, $\mu^{26}Mg^*$ in such inclusions record both a radiogenic ^{26}Mg component related to ^{26}Al decay and a non-radiogenic ^{26}Mg component.

4. Episodic formation of refractory inclusions and their transport to the accretion region of the giant planets

The distinct $\mu^{26}Mg^*_0$ values for bulk refractory inclusions in CV and CR chondrites indicate at least two separate CAI-forming reservoirs/episodes with $(^{26}Al/^{27}Al)_0$ of $\sim 5 \times 10^{-5}$. The three CR

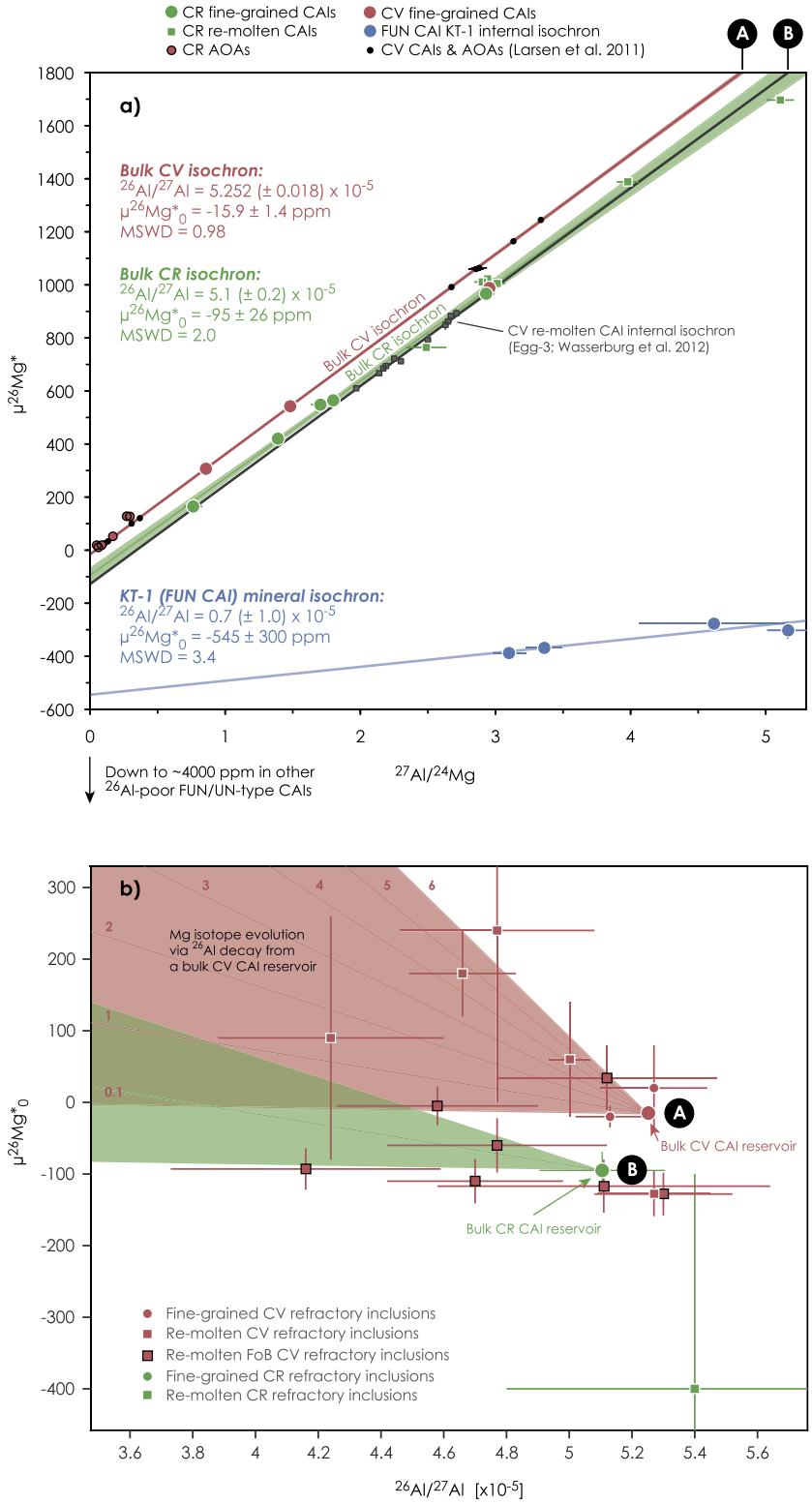

Fig. 1. a) ^{26}Al-^{26}Mg isochron diagram for bulk refractory inclusions from CR and CV chondrites showing the presence of at least two distinct populations of refractory inclusions with significantly different $\mu^{26}Mg^*_0$ (where $\mu^{26}Mg^*_0$ is the intercept of the isochron defined as the parts per million deviation of the initial $^{26}Mg/^{24}Mg$ ratio relative to Earth after mass-dependent fractionation correction using the exponential law and normalization to the solar $^{25}Mg/^{24}Mg$ ratio of 0.126896; Bizzarro et al., 2011). Also shown is the internal mineral isochron for the Egg-3 CV3 CAI from Wasserburg et al., 2012, which coincides with the CR isochron. **b)** Magnesium isotope evolution diagram for refractory inclusions, in which each data point represents the slope ($^{26}Al/^{27}Al$) and intercept ($\mu^{26}Mg^*_0$) in the ^{26}Al-^{26}Mg isochron diagram. The red shaded area represents the range of Mg isotope compositions that can be explained by in-situ ^{26}Al decay from a 'canonical' CV CAI reservoir ($^{26}Al/^{27}Al = 5.25 \times 10^{-5}$ and $\mu^{26}Mg^*_0 = -15.9$ ppm, reservoir A), along trajectories determined by their bulk $^{27}Al/^{24}Mg$ ratios. The green shaded area represents the evolution from a CR CAI reservoir for $^{27}Al/^{24}Mg$ ratios up to 2 typical for forsterite-rich type B (FoB) CAIs. Most CV CAIs (MacPherson et al., 2010; 2012; Kita et al., 2012) can be explained by evolution from the CV reservoir, whereas most FoB CAIs (MacPherson et al., 2016), the type B CAI Egg-3 (Wasserburg et al., 2012) and an igneous CR CAI (Makide et al., 2009) require evolution from a distinct isotope reservoir with deficient $\mu^{26}Mg^*_0$ similar to CR CAIs (reservoir B, this study). Hence, these inclusions belong to a separate population characterized by isotopically anomalous μ^{26} Mg* relative to 'normal' CV CAIs. To facilitate comparison, literature data was recalculated using $\beta = 0.511$. (For interpretation of the colors in the figure(s), the reader is referred to the web version of this article.)

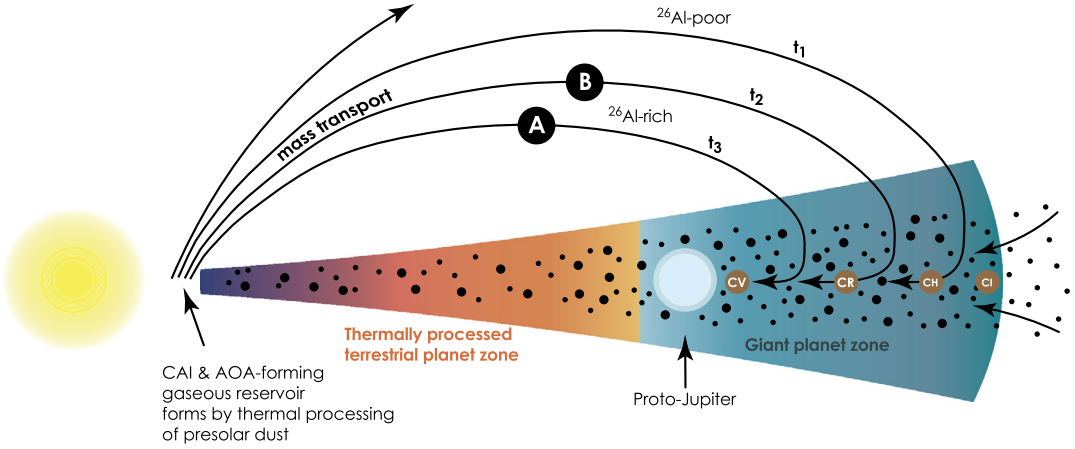

Fig. 2. Disk sketch diagram showing the transport routes and recycling of inner disk refractory material to the accretion regions of the giant planets. ^{26}Al-rich population A inclusions, which represent refractory inclusions from the bulk CV isochron, end up in the accretion region of the CV chondrite parent body close to the orbit of Jupiter, whereas population B inclusions are distributed between the accretion regions of both CV and CR chondrite parent bodies at larger orbital distance. Early-formed ^{26}Al-poor refractory inclusions are transported to larger heliocentric distances to accrete with CH carbonaceous chondrites.

AOAs that plot above the CV isochron cannot be regressed with any other AOAs from this study to define a statistically meaningful regression line. Thus, we speculate that these objects hint at the possibility of yet another population of refractory inclusions with a different initial ^{26}Mg* although additional data is required to test this hypothesis. Thus, the existence of different CAI populations with contrasting $\mu^{26}Mg^*_0$ suggests that formation of ^{26}Al-rich refractory inclusions was a punctuated and recurrent process, plausibly associated with protostellar episodic outbursts from the active proto-Sun (Frimann et al., 2016; Hsieh et al., 2018). Such episodic outbursts are observed for young stellar objects in the process of accreting mass via their disks from the surrounding envelope with episodes lasting for less than a few thousand years (Hsieh et al., 2018), which is consistent with the timeframe deduced from the error envelopes of CV and CR isochrons of <8,000 and <82,000 yr, respectively. Therefore, episodic accretion and CAI-formation may be intrinsically linked, reflecting a generic process inherent to the evolution of protostars.

The presence of CAI material in the comet 81P/Wild 2 has been taken as evidence for CAI transport and recycling into distant regions of the Solar protoplanetary disk (Brownlee et al., 2006). The near absence of such refractory materials in the inner accretion regions of the terrestrial planets (Trinquier et al., 2009; Olsen et al., 2016; Bizzarro et al., 2017) can be explained if refractory inclusions were episodically lofted above the disk midplane and recycled back into the outer disk. Carbonaceous chondrites, such as CV and CR, accreted in the outer volatile-rich part of the disk beyond the orbits of Jupiter, with the CR chondrites most likely accreting at larger heliocentric distances compared to the close proximity of the accretion region of CV chondrites to the orbit of Jupiter (Van Kooten et al., 2016, 2017; Kruijer et al., 2017). If correct, the fact that our new data supports evidence for formation of two distinct populations of refractory inclusions, which now resides in two different types of chondrites (CV and CR), suggests that refractory inclusions belonging to the CV isochron (population A) were predominantly transported to disk regions just beyond Jupiter. On the other hand, population B inclusions (all CR CAIs and some CV CAIs) were present in both the CV and CR accretion regions (Fig. 2). In other words, CR chondrites only captured the inclusions belonging to population B, whereas CV chondrites captured inclusions of both populations A and B. This can be explained if population B inclusions were transported to larger orbital distances than those from population A. Successive inward drift could have introduced inclusions from population B to the CV accretion region, but not vice versa (Fig. 2). Following this reasoning, the high abundance (~85%) and small size of ^{26}Al-poor CAIs in CH chondrites, inferred to have accreted even beyond CR chondrites (Krot et al., 2012) implies that such ^{26}Al-poor inclusions were transported further out in the disk, plausibly at much earlier times. Variable travel distance of refractory inclusions can plausibly be explained by secular changes in the outward transport efficiency of the disk winds associated with episodic outbursts (Audard et al., 2014) and/or size-sorting effects during transport above the disk midplane and subsequently within the outer disk (Hansen, 2014). The latter possibility seems consistent with the size distribution of refractory inclusions in CV and CR chondrites, for which the characteristically large inclusions present in CV chondrites are expected to re-enter the disk midplane at smaller orbital radii, as well as drift faster inwards compared to the much smaller inclusions typical of CR chondrites.

This distribution of refractory inclusions is also consistent with recent numerical simulations showing that an early formation (<1 Myr) of Jupiter can trap CAIs in a pressure maximum beyond it (Desch et al., 2018). In this model, the high abundance of CAIs in CV chondrites is explained by trapping and locally enhancing their modal abundance at the far-Sun side of Jupiter. CR parent bodies accreting at larger orbital distances do not experience this enhancement and consequently contain a lower abundance of CAIs. Apart from the size and abundance differences of refractory inclusions in CV and CR chondrites, the presence of both population A and B in CV chondrites contrasting the apparent exclusive presence of population B in CR chondrites (Figs. 1 and 2) supports this idea. Further, it is generally believed that the isotopically anomalous composition of ^{26}Al-poor inclusions, such as FUN CAIs, requires their formation prior to sufficient isotopic homogenization and admixing of ^{26}Al to the CAI-forming reservoir (Holst et al., 2013). Hence, the predominance of ^{26}Al-poor refractory inclusions at larger heliocentric distances compared to ^{26}Al-rich inclusions suggests that the transport efficiency was progressively decreasing. As such, refractory inclusions record the dynamical evolution of the Solar protoplanetary disk, where populations of inner disk refractory inclusions are periodically lofted above the disk midplane and redistributed to the outer Solar System through large-scale mass transport processes with progressively decreasing efficiency.

5. The presolar heritage of isotopic signatures in refractory inclusions

Through continuous Galactic Chemical Evolution (GCE), stellar nucleosynthesis progressively enriches ^{25}Mg and ^{26}Mg relative to ^{24}Mg in the interstellar medium (Fenner et al., 2003). We note that

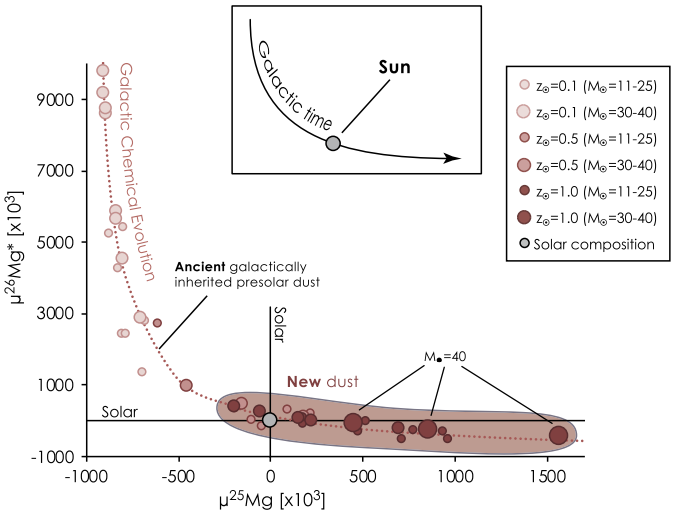

Fig. 3. Galactic chemical evolution (GCE) model and supernova-II (SNII) yields for magnesium isotopes predicted from astrophysical models as a function of stellar mass (M) and metallicity (Z). GCE and SNII yields were extracted from the SNII ejecta tool at the Clemson University web site; URL: http://photon.phys.clemson.edu/gce.html (Meyer et al., 2001). $Z_{\odot}$ refers to solar metallicity and $M_{\odot}$ to solar mass.

this results in an anticorrelation between $^{25}Mg/^{24}Mg$ and $\mu^{26}Mg^*$, trending towards $\mu^{26}Mg^*$ deficits in young dust generations compared to the average dust – a trend which is also corroborated by type-II supernova (SNII) models (Fig. 3). Thus, it appears unavoidable that presolar dust generations of different age on average record divergent Mg-isotope compositions (Clayton, 1988).

Presolar grains from pristine chondritic meteorites are samples of the molecular cloud dust that made up our Solar System. We find that the presolar grain data for graphites, silicates and oxides agree with the theoretical predictions from GCE and SNII models for an anticorrelation between $^{25}Mg/^{24}Mg$ and $\mu^{26}Mg^*$, thereby reflecting the galactically inherited non-radiogenic $^{26}Mg^*$ background (Fig. 4a). Nucleosynthetic addition of ^{26}Al would produce a radiogenic spike in its decay product $^{26}Mg^*$ in young dust through radioactive decay, thereby overprinting this galactic background. Indeed, a clear $^{26}Mg^*$ spike is observed for presolar grains with about solar $^{25}Mg/^{24}Mg$. This is most noticeably in low-density presolar graphite grains believed to originate from SNII (Lodders and Amari, 2005) and group 3 and 4 oxide grains originating from either SNII or low-mass and low-metallicity Asymptotic Giant Branch (AGB) stars (Lodders and Amari, 2005; Nittler et al., 2008) (Fig. 4a). It is also consistent with the Mg-isotope systematics in SNII presolar SiC grains of the X type (Lodders and Amari, 2005). Thus, the presolar grain record demonstrates a mutual exclusivity between large $^{25}Mg/^{24}Mg$ excesses (coupled with μ^{26} Mg^* deficits) and evidence for ^{26}Al, and reveal three main dust components/generations; 1) an ancient galactically inherited component with excess μ^{26} Mg^* (coupled with deficit $^{25}Mg/^{24}Mg$), 2) a newer molecular cloud component with deficit $\mu^{26}Mg^*$ (coupled with excess $^{25}Mg/^{24}Mg$), and 3) a young ^{26}Al-rich component with about solar non-radiogenic $\mu^{26}Mg^*$ (coupled with about solar $^{25}Mg/^{24}Mg$) (Fig. 4a inset). Hence, if refractory inclusions indeed formed by incomplete vaporization of such dust components, they are predicted to capture diluted signatures of its isotopically anomalous compositions. The distinct Mg-isotopic signatures of refractory inclusions reported here indicate progressive admixing of exotic presolar dust to the hot inner disk CAI-forming region.

For example, a characteristic feature of FUN-type CAIs is the presence of large mass-independent nucleosynthetic isotope effects in ^{48}Ca, ^{50}Ti and ^{54}Cr, as well as $^{26}Mg^*$ deficits coupled with the general lack of evidence for the former presence of ^{26}Al (Schiller et al., 2015; Kööp et al., 2018; Lee et al., 1979; Holst et al., 2013). The KT-1 FUN CV CAI reported here ($\mu^{26}Mg^*_0 = -545 \pm 300$ ppm, $[^{26}Al/^{27}Al]_0 < 1.7 \times 10^{-5}$) is an example of this. Although the extreme $^{25}Mg/^{24}Mg$ enrichments typical for FUN-type refractory inclusions could in principle be explained by kinetic mass-dependent fractionation effects (Davis et al., 2015), these processes cannot account for their large μ^{26} Mg^* deficits, down to ~−4000 ppm (Makide et al., 2009; Kööp et al., 2016), and not either those observed in ^{26}Al-poor PLAC-type CAIs (Liu et al., 2009; Kööp et al., 2016). This is because the range of beta values (0.511-0.513) experimentally determined for Mg isotope fractionation through evaporation of such CAI compositions cannot account for such large deficits (e.g. Davis et al., 2015). Instead, we propose that these features can be explained if FUN- and PLAC-type refractory inclusions formed from a gas dominated by vaporized new, but ^{26}Al-poor (i.e. >10 Myr prior to Solar System formation), presolar dust characterized by $\mu^{26}Mg^*$ deficits (component 2 in Fig. 4a). As such, these types of CAI's may represent a diluted signature of the more extreme presolar component 2, for which FUN-type inclusions potentially record a secondary mass-fractionation overprint (Fig. 4b).

On the other hand, ^{26}Al-rich refractory inclusions [with $(^{26}Al/^{27}Al)_0$ of $\sim 5 \times 10^{-5}$], such as 'normal' CV CAIs and SHIB-type (Spinel-HIBonite inclusions) CAIs in CM chondrites lack the extreme nucleosynthetic effects seen in FUN/UN CAIs and PLACs (Fig. 3b), thereby mirroring the mutual exclusivity between ^{26}Al and $\mu^{26}Mg^*$ deficits recorded by presolar grains (Fig. 4). The formation of ^{26}Al-rich refractory inclusions can be explained by their formation from a gas dominated by vaporized young dust (component 3 in Fig. 4a inset) rich in ^{26}Al and of roughly solar non-radiogenic $\mu^{26}Mg^*$ and solar $^{25}Mg/^{24}Mg$. Thus, these ^{26}Al-rich CAI types seem to represent diluted signatures of the more extreme presolar component 3. If this dust originated from SNII ejecta in the protosolar molecular cloud, as indicated by the presolar grain record (Fig. 4a), we find that the average free-decay age of this dust, resulting from the difference between the $(^{26}Al/^{27}Al)_0$ ratio of $\sim 5 \times 10^{-5}$ in 'normal' CAIs and the average $(^{26}Al/^{27}Al)_0$ yields of $\sim 5 \times 10^{-3}$ from SNII nucleosynthesis models of solar metallicity massive stars ($M_{\odot} = 30 - 35$) with near solar $^{25}Mg/^{24}Mg$ (Fig. S11 in the supplementary material), is less than 5 Myr depending on the relative proportion of SNII-derived ^{26}Al in CAIs. Hence, this dust was less than 5 Myr old on average when it became incorporated into ^{26}Al-rich CAIs.

Finally, we note that all of the fine-grained CR CAI condensates measured in this study record solar to super-solar $^{25}Mg/^{24}Mg$ (up to ~ 800 ppm; Table 1). This is unexpected from theoretical predictions for condensation from a solar composition gas, in which the lighter isotopes are preferentially partitioned into the condensate (Davis and Richter, 2014). This suggests that the CR CAI-forming gas was characterized by a slight enrichment in $^{25}Mg/^{24}Mg$ (>800 ppm) and deficit in $\mu^{26}Mg^*_0$ (<−5 ppm) relative to the average solar composition. This further mirrors the anticorrelated $^{25}Mg/^{24}Mg$ and $\mu^{26}Mg^*_0$ observed for the presolar grains record and suggest that the CR CAI-forming gas was of slightly non-solar composition generated via preferential selective admixing of isotopically anomalous young dust components (2 & 3).

6. Thermal processing and the distribution of Mg isotopes and ^{26}Al in the early Solar System

The CAI-forming gas was generated by thermal processing of presolar dust accreting to the proto-Sun. However, the presence of widespread nucleosynthetic isotope anomalies in a range of elements (e.g., Mg, Al, Cr, Ca, Ti) in refractory inclusions is not compatible with a homogeneous solar composition gas (Ireland, 1990).

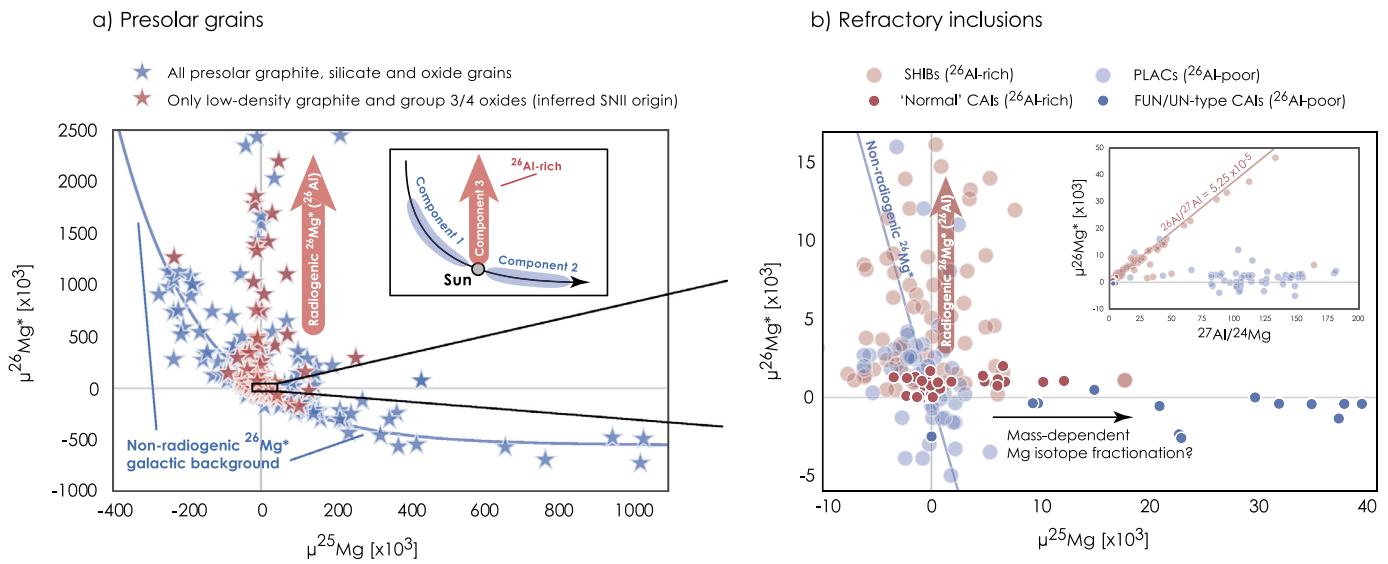

Fig. 4. μ^{25}Mg (^{25} Mg/^{24} Mg) versus μ^{26}Mg* diagrams similar to Fig. 3. **a)** Magnesium isotope composition of presolar grains extracted from the presolar grain database (Hynes and Gyngard, 2009); the curved line defines an exponential fit to presolar silicates (low Al/Mg) representing the non-radiogenic ^{26}Mg component (no radiogenic ^{26}Mg from ^{26}Al decay). **b)** Magnesium isotope systematics of refractory inclusions in chondritic meteorites, incl. 'normal' CV/CR, FUN/UN, SHIBs and PLACs. Inclusions marked in red ('normal' CV/CR CAIs and SHIBs) record clear evidence for the former presence of ^{26}Al by correlated δ^{26}Mg* (radiogenic) and Al/Mg excesses (inset), whereas inclusions marked in blue (FUN/UN CAIs and PLACs) shows no evidence for ^{26}Al with many recording resolvable δ^{26}Mg* deficits. Inset shows the ^{26}Al-^{26}Mg isochron diagram for the same types of refractory inclusions, demonstrating the radiogenic contribution on ^{26} Mg* from ^{26}Al decay in SHIBs and 'normal' CAIs at an initial ^{26}Al/^{27}Al ratio of ~5.25 × 10^{-5}. SHIBs = Spinel-HIBonite inclusions, PLACs = PLAty hibonite Crystals, FUN = Fractionation and Unknown Nuclear effects.

As such, dust sublimation was incomplete prior to formation of these solids. We infer that this gas composition was governed by the thermal properties of isotopically anomalous presolar carriers. Our analysis suggests that populations of refractory inclusions formed through episodic transient heating events, thereby capturing distinct snapshots of an isotopically evolving CAI-forming reservoir. Some CAIs (PLACs and FUN/UN CAIs) clearly preserved nucleosynthetic 'nugget' effects (% range for ^{48}Ca and ^{50}Ti [Kööp et al., 2018]) from refractory oxide residues rich in Ca and Ti (e.g., presolar hibonite and corundum), whereas nucleosynthetic effects in more volatile elements, such as Mg (enriched in presolar silicates such as pyroxene and olivine), were significantly reduced (^{26}Mg*$_0$ < 0.5‰; Fig. 4b). These observations corroborate a volatility-controlled sublimation of mineralogically diverse presolar carriers, implying a closer to solar isotope composition in the gas for volatile elements, such as Mg, than those of refractory elements such as Ca and Ti.

Extraction of new dust components (2 & 3), carrying μ^{26}Mg* deficits and ^{26}Al/^{27}Al enrichments, into the CAI-forming gas suggests a relatively volatile mineralogy. This generates a complementarity in the residual thermally processed midplane dust in the inner protoplanetary disk, resulting in a net non-radiogenic μ^{26}Mg* excess coupled with a ^{25}Mg/^{24}Mg and ^{26}Al/^{27}Al deficit relative to the solar average (Fig. 5). This dust accretes to form the terrestrial planets, thereby providing a mechanism for explaining the reduced initial $(^{26}Al/^{27}Al)_0$ in the inner solar protoplanetary disk relative to CI chondrites (Larsen et al., 2011; 2016; Schiller et al., 2015). The μ^{26}Mg* deficit recorded by inner Solar System bodies (such as ordinary chondrites and angrites (Larsen et al., 2011)) can therefore only be explained by a reduced radiogenic ^{26}Mg* ingrowth relative to the solar average represented by CI chondrites (Fig. 5 and Fig. S12 in the supplementary material).

We conclude that the Mg-isotope systematics of the Solar System can be justified by chemical unmixing by thermal processing of the three molecular cloud components; 1) an ancient galactically inherited and thermally resilient ^{26}Al-poor presolar dust component enriched in non-radiogenic ^{26}Mg*, which became enriched in the inner terrestrial planet-forming region by virtue of loss of some of the other components, 2) a newer ^{26}Al-poor thermally

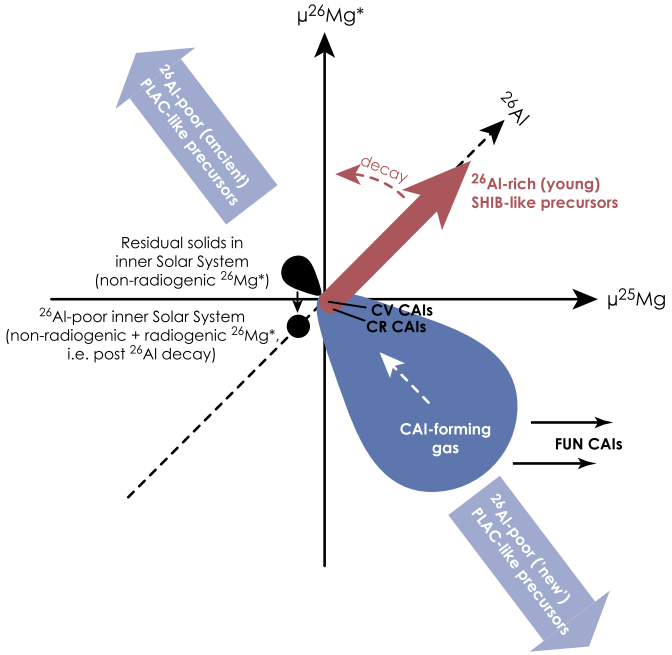

Fig. 5. δ^{25}Mg versus δ^{26}Mg* diagram (similar to Fig. 3 and 4, but with a 3rd dimension representing ^{26}Al) showing the predicted complementarity between the CAI-forming gas and residual midplane solids formed through progressive thermal processing of isotopically anomalous presolar carriers. Sublimation of thermally labile presolar carriers (e.g., silicates) from a relatively new generation of presolar dust (solar metallicity, component 2) generates a gaseous reservoir enriched in ^{25}Mg/^{24}Mg and deficient in μ^{26}Mg*. ^{26}Al-poor FUN-type CAIs form from this reservoir. Subsequent higher-temperature sublimation of ^{26}Al-rich young presolar carriers with about solar ^{25}Mg/^{24}Mg (e.g., oxides) enriches the gas in ^{26}Al from which 'normal' ^{26}Al-rich CV/CR CAIs form. The complimentary residual solids become depleted in these components (^{26}Al-depleted) and accretes to form the terrestrial planets. This effect generates a non-radiogenic μ^{26}Mg* excess combined with a radiogenic μ^{26}Mg* deficit [from a reduced initial $(^{26}Al/^{27}Al)_0$] in the terrestrial planet-forming region as compared to the Solar average, i.e. a net μ^{26}Mg* deficit relative to CI chondrites after ^{26}Al decay as represented by the black dot. The dotted line is the 3rd dimension representing ^{26}Al. Decay of ^{26}Al to ^{26}Mg (1:1) is shown by the dotted red curved arrow.

labile dust component deficient in non-radiogenic $^{26}Mg^{*}$, plausibly inherited from the proto-solar molecular cloud >10 Myr prior to Solar System formation, which is recorded in FUN/UN/PLAC-type CAIs, and 3) a freshly synthesized (on average <5 Myr old) ^{26}Al-rich molecular cloud component, which was enriched in the CAI-forming gas and subsequently incorporated into ^{26}Al-rich refractory inclusions, such as 'normal' CV, CR and SHIB-type CAIs.

Declaration of competing interest

The authors declare that they have no known competing financial interests or personal relationships that could have appeared to influence the work reported in this paper.

Acknowledgements

Funding for this project was provided by grants from the Danish National Research Foundation (grant number DNRF97) and from the European Research Council (ERC Consolidator grant agreement 616027-STARDUST2ASTEROIDS) to M.B. We thank Rajdeep Dasgupta for careful editorial handling of our manuscript, as well as Andrew Davis and an anonymous reviewer for constructive comments and suggestions which improved the clarity of our interpretations.

Appendix A. Supplementary material

Supplementary material related to this article can be found online at https://doi.org/10.1016/j.epsl.2020.116088.

References

Audard, M., et al., 2014. Episodic accretion in young stars. In: Protostars and Planets VI, pp. 1–24.
Bizzarro, M., et al., 2011. High-precision Mg-isotope measurements of terrestrial and extraterrestrial material by HR-MC-ICPMS—implications for the relative and absolute Mg-isotope composition of the bulk silicate Earth. J. Anal. At. Spectrom. 26 (3), 565.
Bizzarro, M., Connelly, J.N., Krot, A.N., 2017. Chondrules: ubiquitous chondritic solids tracking the evolution of the solar protoplanetary disk. In: Formation, Evolution and Dynamics of Young Solar Systems. In: Astrophysics and Space Science Library. Springer International Publishing, Cham, pp. 161–195.
Brownlee, D., et al., 2006. Comet 81P/Wild 2 under a microscope. Science 314 (5806), 1711–1716.
Clayton, D.D., 1988. Isotopic anomalies: chemical memory of Galactic evolution. Astrophys. J. 334, 191–195.
Connelly, J.N., et al., 2012. The absolute chronology and thermal processing of solids in the solar protoplanetary disk. Science 338, 651–655.
D'Alessio, P., Calvet, N., Woolum, D.S., 2005. Thermal structure of protoplanetary disks. In: Krot, A.N., Scott, E.R.D., Reipurth, B. (Eds.), Chondrites and the Protoplanetary Disk. In: ASP Conference Series, vol. 341, pp. 353–372.
Davis, A.M., Richter, F.M., 2014. Condensation and evaporation of solar system materials. In: Davis, A.M. (Ed.), Meteorites and Cosmochemical Processes. In: Treatise on Geochemistry, 2nd Ed., vol. 1. Elsevier, Oxford, pp. 335–360. H.D. Holland and K.K. Turekian (Exec. Eds.).
Davis, A.M., et al., 2015. Isotopic mass fractionation laws for magnesium and their effects on ^{26}Al–^{26}Mg systematics in solar system materials. Geochim. Cosmochim. Acta 158, 245–261.
Desch, S.J., Kalyaan, A., Alexander, C.M.O., 2018. The effect of Jupiter's formation on the distribution of refractory elements and inclusions in meteorites. Astrophys. J. Suppl. Ser. 238 (11), 1–31.
Fenner, Y., et al., 2003. The chemical evolution of magnesium isotopic abundances in the solar neighbourhood. Publ. Astron. Soc. Aust. 20 (04), 340–344.
Frimann, S., Jorgensen, J.K., Padoan, P., Haugbølle, T., 2016. Protostellar accretion traced with chemistry. Astron. Astrophys. 587 (A60), 1–11.
Hansen, B.M.S., 2014. The circulation of dust in protoplanetary discs and the initial conditions of planet formation. Mon. Not. R. Astron. Soc. 440 (4), 3545–3556.
Holst, J., et al., 2013. ^{182}Hf-^{182}W age dating of a ^{26}Al-poor inclusion and implications for the origin of short-lived radioisotopes in the early Solar System. Proc. Natl. Acad. Sci. USA 110 (22), 8819–8823.
Hsieh, T-H., et al., 2018. Probing episodic accretion in very low luminosity objects. Astrophys. J. 854 (15), 1–29.
Hynes, K.M., Gyngard, F., 2009. The Presolar Grain Database: http://presolar.wustl.edu/~pgd. In: Lunar and Planetary Science Conference XL. Abstract 1198.
Ireland, T.R., 1990. Presolar isotopic and chemical signatures in hibonite-bearing refractory inclusions from the Murchison carbonaceous chondrite. Geochim. Cosmochim. Acta 54 (11), 3219–3237.
Kita, N.T., et al., 2012. Internal ^{26}Al-^{26}Mg isotope systematics of a Type B CAI: remelting of refractory precursor solids. Geochim. Cosmochim. Acta 86, 37–51.
Kita, N.T., Yin, Q.-Z., MacPherson, G.J., Ushikubo, T., Jacobsen, B., Nagashima, K., Kurahashi, E., Krot, A.N., Jacobsen, S.B., 2013. ^{26}Al-^{26}Mg isotope systematics of the first solids in the early solar system. Meteorit. Planet. Sci., 1–18.
Kööp, L., et al., 2016. A link between oxygen, calcium and titanium isotopes in ^{26}Al-poor hibonite-rich CAIs from Murchison and implications for the heterogeneity of dust reservoirs in the solar nebula. Geochim. Cosmochim. Acta 189:70–95.
Kööp, L., et al., 2018. A multielement isotopic study of refractory FUN and F CAIs: mass-dependent and mass-independent isotope effects. Geochim. Cosmochim. Acta 221, 296–317.
Krot, A.N., Meibom, A., Weisberg, M.K., Keil, K., 2002. The CR chondrite clan: implications for early solar system processes. Meteorit. Planet. Sci. 37 (11), 1451–1490.
Krot, A.N., et al., 2012. Heterogeneous distribution of ^{26}Al at the birth of the solar system: evidence from refractory grains and inclusions. Meteorit. Planet. Sci. 47 (12), 1948–1979.
Kruijer, T.S., Burkhardt, C., Budde, G., Kleine, T., 2017. Age of Jupiter inferred from the distinct genetics and formation times of meteorites. Proc. Natl. Acad. Sci. USA 114, 6712–6716.
Kuffmeier, M., Mogensen, T.F., Haugbølle, T., Bizzarro, M., Nordlund, Å, 2016. Tracking the distribution of ^{26}Al and ^{60} Fe during the early phases of star and disk evolution. Astrophys. J. 826 (1), 22.
Larsen, K.K., et al., 2011. Evidence for magnesium isotope heterogeneity in the solar protoplanetary disk. Astrophys. J. Lett. 735 (2), L37.
Larsen, K.K., Schiller, M., Bizzarro, M., 2016. Accretion timescales and style of asteroidal differentiation in an 26Al-poor protoplanetary disk. Geochim. Cosmochim. Acta 176, 295–315.
Larsen, K.K., Wielandt, D., Bizzarro, M., 2018. Multi-element ion-exchange chromatography and high-precision MC-ICP-MS isotope analysis of Mg and Ti from sub-mm-sized meteorite inclusions. J. Anal. At. Spectrom. 33 (4), 613–628.
Lee, T., Russell, W.A., Wasserburg, G.J., 1979. Calcium isotopic anomalies and the lack of aluminum-26 in an unusual Allende inclusion. Astrophys. J. Lett. 228, L93–L98.
Liu, M-C., et al., 2009. Isotopic records in CM hibonites: implications for timescales of mixing of isotope reservoirs in the solar nebula. Geochim. Cosmochim. Acta 73 (17), 5051–5079.
Lodders, K., Amari, S., 2005. Presolar grains from meteorites: remnants from the early times of the solar system. Chem. Erde - Geochem. 65 (2), 93–166.
MacPherson, G.J., et al., 2010. Early nebula condensates with canonical, not supracanonical, initial $^{26}Al/^{27}Al$ ratios. Astrophys. J. Lett. 711 (2), L117–L121.
MacPherson, G.J., Kita, N.T., Ushikubo, T., Bullock, E.S., Davis, A.M., 2012. Well-resolved variations in the formation ages for Ca–Al-rich inclusions in the early Solar System. Earth Planet. Sci. Lett. 331–332, 43–54.
MacPherson, G.J., 2014. Calcium–aluminum-rich inclusions in chondritic meteorites. In: Treatise on Geochemistry. Elsevier Ltd., pp. 139–179.
MacPherson, G.J., et al., 2016. High precision Al-Mg systematics of forsterite-bearing type B CAIs from CV3 chondrites. Geochim. Cosmochim. Acta, 1–42.
Makide, K., et al., 2009. Oxygen- and magnesium-isotope compositions of calcium–aluminum-rich inclusions from CR2 carbonaceous chondrites. Geochim. Cosmochim. Acta 73 (17), 5018–5050.
Meyer, B.S., Denny, J.E., Clayton, D.D., 2001. Calculating chemical evolution on the Web. In: Lunar and Planetary Science Conference XXXII. Abstract 1785.
Nittler, L.R., et al., 2008. Aluminum-, calcium- and titanium-rich oxide stardust in ordinary chondrite meteorites. Astrophys. J. 682 (2), 1450–1478.
Olsen, M.B., Schiller, M., Krot, A.N., Bizzarro, M., 2013. Magnesium isotope evidence for single stage formation of CB chondrules by colliding planetesimals. Astrophys. J. Lett. 776 (1), L1.
Olsen, M.B., Wielandt, D., Schiller, M., Van Kooten, E.M.M.E., Bizzarro, M., 2016. Magnesium and ^{54} Cr isotope compositions of carbonaceous chondrite chondrules – insights into early disk processes. Geochim. Cosmochim. Acta 191, 118–138.
Paton, C., Hellstrom, J., Paul, B., Woodhead, J., Hergt, J., 2011. Iolite: freeware for the visualisation and processing of mass spectrometric data. J. Anal. At. Spectrom. 26 (12), 2508.
Paton, C., Schiller, M., Ulfbeck, D., Bizzarro, M., 2012. High-precision $^{27}Al/^{24}Mg$ ratio determination using a modified isotope-dilution approach. J. Anal. At. Spectrom. 27 (4), 644.
Schiller, M., Paton, C., Bizzarro, M., 2015. Evidence for nucleosynthetic enrichment of the protosolar molecular cloud core by multiple supernova events. Geochim. Cosmochim. Acta 149 (C), 88–102.
Schiller, M., Bizzarro, M., Fernandes, V.A., 2018. Isotopic evolution of the protoplanetary disk and the building blocks of Earth and the Moon. Nature 555 (7697), 507–510.
Scott, E.R.D., Krot, A.N., 2014. Chondrites and their components. In: Davis, A.M. (Ed.), Meteorites and Cosmochemical Processes. In: Treatise on Geochemistry, 2nd Ed., vol. 1. Elsevier, Oxford, pp. 65–137. H.D. Holland and K.K. Turekian (Exec. Eds.).

Simon, S.B., Grossman, L., 2006. A comparative study of melilite and fassaite in Types B1 and B2 refractory inclusions. Geochim. Cosmochim. Acta 70 (3), 780–798.

Sossi, P.A., et al., 2017. Early Solar System irradiation quantified by linked vanadium and beryllium isotope variations in meteorites. Nat. Astron. 1, 0055.

Thrane, K., Nagashima, K., Krot, A.N., Bizzarro, M., 2008. Discovery of a new FUN CAI from a CV carbonaceous chondrite: evidence for multistage thermal processing in the protoplanetary disk. Astrophys. J. Lett. 680 (2), L141.

Trinquier, A., et al., 2009. Origin of nucleosynthetic isotope heterogeneity in the solar protoplanetary disk. Science 324 (5925), 374–376.

Van Kooten, E.M.M.E., et al., 2016. Isotopic evidence for primordial molecular cloud material in metal-rich carbonaceous chondrites. Proc. Natl. Acad. Sci. USA 113 (8), 2011–2016.

Van Kooten, E.M.M.E., Schiller, M., Bizzarro, M., 2017. Magnesium and chromium isotope evidence for initial melting by radioactive decay of Al and late stage impact-melting. Geochim. Cosmochim. Acta 208, 1–23.

Vasileiadis, A., Nordlund, A., Bizzarro, M., 2013. Abundance of ^{26}Al and ^{60}Fe in evolving Giant Molecular Clouds. Astrophys. J. Lett. 769, L8.

Warren, P.H., 2011. Stable-isotopic anomalies and the accretionary assemblage of the Earth and Mars: a subordinate role for carbonaceous chondrites. Earth Planet. Sci. Lett. 311 (1–2), 93–100.

Wasserburg, G.J., Wimpenny, J., Yin, Q-Z., 2012. Mg isotopic heterogeneity, Al-Mg isochrons, and canonical ^{26}Al/^{27}Al in the early solar system. Meteorit. Planet. Sci. 47 (12), 1980–1997.

Wielandt, D., et al., 2012. Evidence for multiple sources of ^{10}Be in the early solar system. Astrophys. J. Lett. 748 (L25), 1–7.